ACS Catalysis

Letter

pubs.acs.org/acscatalysis

Photothermal Hydrogen Production Using Noble-Metal-Free Ti@TiO_2 Core−Shell Nanoparticles under Visible−NIR Light Irradiation

Sergey I. Nikitenko,*[,†] Tony Chave,[†] Camille Cau,[†] Henri-Pierre Brau,[†] and Valérie Flaud[‡]

[†]Institut de Chimie Séparative de Marcoule (ICSM), UMR 5257−CEA−CNRS−UM−ENSCM, Centre de Marcoule, Bat. 426, BP 17171, 30207 Bagnols sur Cèze, Cedex, France

[‡]Institut de Chimie Moléculaire et des Matériaux de Montpellier UMR 5253, Université Montpellier, Place Eugène Bataillon, Bat. 15, 34095 Montpellier Cedex 5, France

Supporting Information

ABSTRACT: Limiting resources of fossil fuels and environmental issues inevitably require more efficient utilization of solar energy. Photocatalytic production of hydrogen is identified as one of the most promising routes for developing clean and sustainable energy; however, engineering low-cost materials exhibiting high catalytic activity in the entire range of the solar spectrum is still a challenge. Here, for the first time, we report simple, easily scalable, and environmentally friendly synthesis of stable Ti@TiO_2 core−shell nanoparticles exhibiting photocatalytic activity in hydrogen production under vis/NIR light irradiation without any noble metals. Stable to oxidation core−shell Ti@TiO_2 nanoparticles have been obtained by the simultaneous actions of ultrasound and hydrothermal treatment on air-passivated titanium metal nanoparticles in pure water. The obtained material is composed of quasi-spherical Ti particles (20−80 nm) coated by 5−15 nm crystals of defect-free anatase with small amounts of rutile. In contrast to pristine TiO_2, the Ti@TiO_2 nanoparticles extend the photo response from the UV to the NIR light region as a result of the light absorption by a nonplasmonic Ti core. In MeOH−H_2O solutions, the Ti@TiO_2 nanoparticles exhibit the strongest catalytic activity in H_2 formation under joint effect of vis/NIR light and heat. Isotopic study using MeOH−D_2O solutions suggests a reaction mechanism involving electron holes' accumulation in a semiconducting TiO_2 shell via charge separation and multiple charge-transfer steps that follow Ti interband transition. The electron transport from the Ti core presumably occurs through the junctions between the TiO_2 crystals at the surface of core−shell nanoparticles.

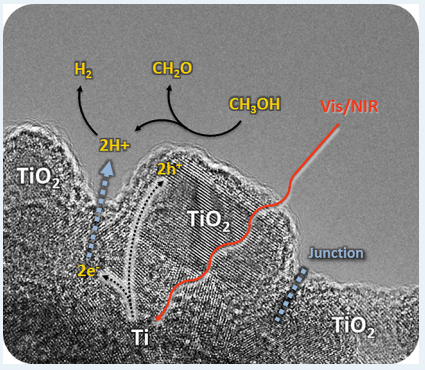

KEYWORDS: *photocatalysis, hydrogen production, titanium nanoparticles, vis/NIR light, solar energy*

The Sun delivers to the Earth's surface ~1.5×10^{18} kWh of energy per year, mostly in the form of visible (vis) and near-infrared (NIR) light. Photocatalytic generation of hydrogen is considered as one of the most promising route to use this abundant energy for environmentally friendly, clean technologies. Among a large variety of photocatalysts studied in recent decades, titanium dioxide (TiO_2) has attracted much attention due to low cost, low toxicity, and good chemical and thermal stability.[1−4] However, TiO_2 can absorb only around 6% of the sunlight. Moreover, about 90% of the electron−hole pairs photogenerated in TiO_2 semiconductor recombine within 10 ns, which strongly reduces its overall quantum efficiency.[5] Incorporation of an electron sink, such as Pt, Au, or Ru, greatly improves the photocatalytic activity of TiO_2;[3,4] however, noble metals are scarce elements and will be too expensive for large-scale utilization in the near future. Solar absorption of TiO_2 can be increased by doping with various cationic and anionic species.[4] For instance, incorporation of Ti(III) ions into the TiO_2 structure allowed optical absorption shifts from the UV to vis spectral range.[6,7] Nevertheless, loading of Pt or Au is still required for these materials[7,8] because doping of TiO_2 creates charge recombination defect sites leading to the drop in the hydrogen yield.

In principal, the development of metallic core/TiO_2 shell particles offers the possibility to solve this critical issue. For instance, Ag@TiO_2 nanoparticles demonstrated substantial photocatalytic activity under UV irradiation as a result of the accumulation of the electrons photogenerated by TiO_2 in the metallic Ag core and their discharge in the presence of electron acceptors.[9] More recently, it was reported that TiO_2-coated titanium nanorods exhibit enhanced photocurrent efficiency in the vis region compared with pristine TiO_2 nanotubes.[10] Here, for the first time, we report a simple and environmentally friendly synthesis of Ti@TiO_2 core−shell nanoparticles exhibiting strong photothermal catalytic activity in the reaction of hydrogen generation under vis/NIR light irradiation in the absence of any noble metals.

Commercially available titanium metal nanoparticles are oxygen- and water-sensitive and therefore cannot be employed in catalysis as such. In this work, a stable Ti@TiO_2

Received: January 28, 2015
Published: July 15, 2015

DOI: 10.1021/acscatal.5b01401
ACS Catal. 2015, 5, 4790−4795

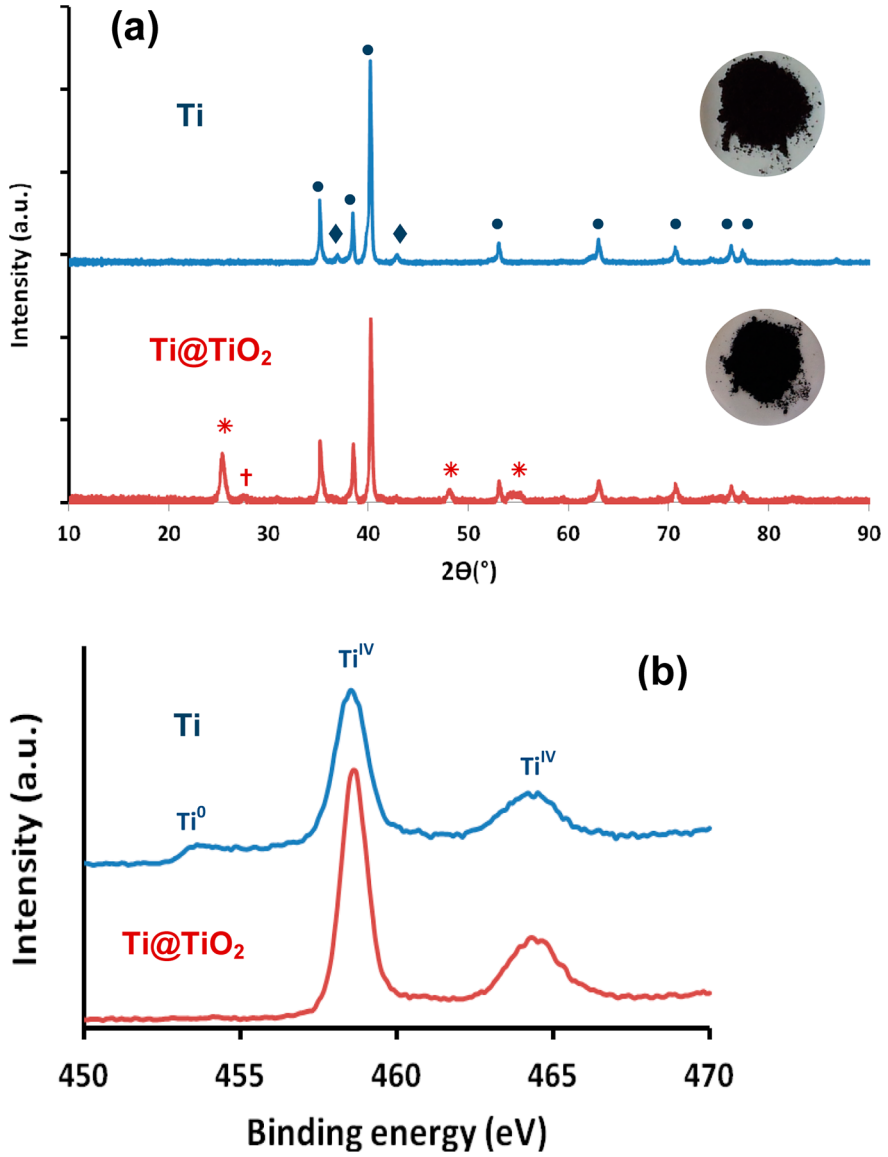

Figure 1. Structural and chemical characterization of titanium nanoparticles before and after sonohydrothermal treatment. Powder XRD of passivated (Ti) and SHT-treated (Ti@TiO_2) particles, Ti (●), TiH_x (◆), anatase (*), rutile (†) (a) and Ti 2p high resolution XPS spectra for these materials (b).

photocatalyst was obtained in two stages: (i) primary passivation of Ti nanopowder and (ii) crystallization of TiO_2 nanoparticles at the surface of the metallic Ti core. The passivation was performed simply by storage of Ti nanopowder in contact with air at room temperature for at least 48 h. The second stage consisted in the hydrothermal treatment of passivated Ti powder in pure water (200 °C, 13 bar, 6 h) coupled with the simultaneous irradiation by power ultrasound (20 kHz, P_{ac} = 10 W). Recently, it was shown that such a sonohydrothermal treatment (SHT) accelerates the crystallization and improves the catalytic performance of nanocrystalline metal oxides.[11] The experimental details about the SHT reactor are presented in the Supporting Information (Figure S1).

The passivated Ti particles exhibit XRD patterns of metallic titanium with admixtures of tetragonal titanium hydride TiH_x (x = 1.53−1.97) (Figure 1a), which is typical for commercial titanium powders.[12] SHT treatment causes appearance of anatase and small amounts of rutile in addition to metallic titanium. By contrast, the intensity of titanium hydride patterns is strongly reduced. Note here that both passivated and SHT powders preserve the intense black color of the initial nanopowder. The high resolution Ti 2p XPS spectrum of passivated Ti particles (Figure 1b) shows the presence of Ti(IV) (464.8 and 458.5 eV, 15.8 at. %) and Ti^0 (453.6 eV, at. 1.7%) at the surface. The signal of Ti^0 disappears after SHT treatment, indicating an effective coating of the metallic titanium surface. In addition, defect states as Ti(II) (455.3 and 461.7 eV) or Ti(III) (457.0 and 463.1 eV) are not observed. Comparison of XRD patterns and XPS spectra allows one to conclude that the passivated Ti is coated by amorphous Ti(IV) species, in contrast to a crystallized TiO_2 shell at the surface of SHT particles. According to TGA/DSC data shown in the Supporting Information (Figure S4), the content of titanium oxide increases from 13 mol % in passivated Ti to 24 mol % in Ti@TiO_2. This implies that formation of the nanocrystalline titanium oxide shell during SHT treatment involves two stages: crystallization of amorphous titanium oxide

DOI: 10.1021/acscatal.5b01401
ACS Catal. 2015, 5, 4790−4795

presented in passivated Ti and partial oxidation of metallic titanium under hydrothermal conditions.

The typical TEM image of passivated Ti (Figure 2a) demonstrates quasi-spherical metallic particles with a diameter

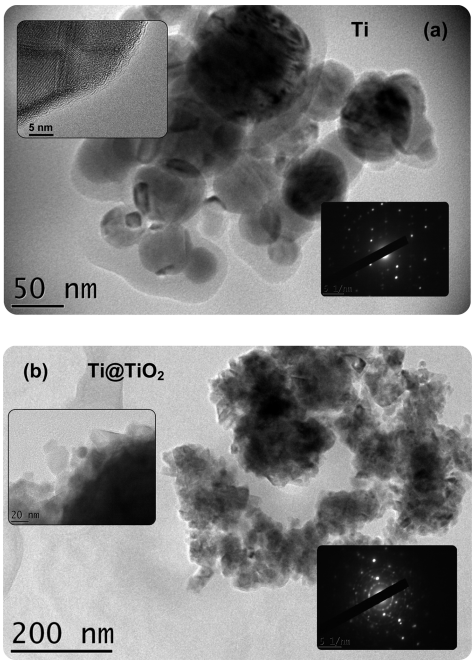

Figure 2. Typical TEM images of titanium nanoparticles before and after sonohydrothermal treatment. (a) Passivated Ti particles. (b) Ti@TiO_2 particles.

in the range of 20−80 nm and without any crystalline oxide shell, in agreement with the XRD analysis. As can be observed from Figure 2b, SHT treatment leads to the formation of 5−15 nm crystals coating the metallic surface. The electron diffraction data are in agreement with formation of a new crystalline phase. Note here that the titanium core preserves its spherical morphology during the coating. According to XRD, the nanocrystalline shell consists principally of anatase with small admixtures of rutile. A solid-state reflectance spectrum of passivated Ti (Figure 3) shows a broad continuum in the UV/vis/NIR spectral range resulting from optical excitation of metallic Ti electronic interband transitions.[13] The amorphous titanium oxide at the surface of passivated Ti particles does not exhibit any specific adsorption bands; however, the spectrum of SHT-treated Ti@TiO_2 particles reveals an absorption band centered at 308 nm that is due to the bandgap transition of

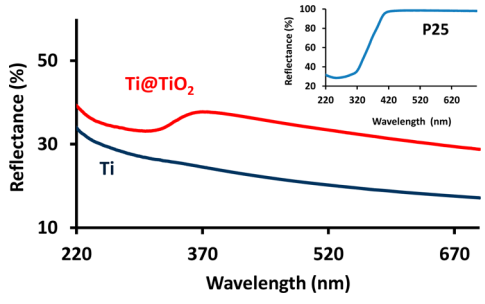

Figure 3. Solid-state reflectance spectra of passivated Ti and core−shell Ti@TiO_2 particles. Inset shows the spectrum of commercial P25 titanium oxide.

crystallized TiO_2. The bandgap energy calculated for Ti@TiO_2 by applying the Kubelka−Munk model as a $(F(R)h\nu)^{1/2}/E$ plot[13] (Figure 4) is equal to 3.28 eV, which is very similar to the

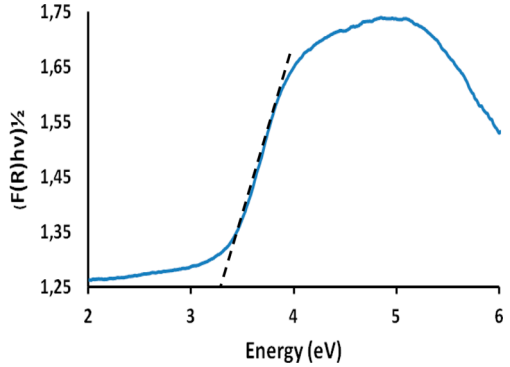

Figure 4. Graphical representation of Kubelka−Munk treatment for Ti@TiO_2 particles.

pristine anatase bandgap energy (3.25 eV).[14] On the other hand, Figure 3 clearly shows that in contrast to commercial P25, the Ti@TiO_2 material extends the photo response from the UV to the NIR light region that makes more efficient use of the solar spectrum. It is worth noting that the obtained bandgap energy indicates the absence of defects in the TiO_2 nanocrystalline shell because usually, the introduction of dopants causes a bandgap narrowing. For instance, TiO_2 self-doped with Ti(III), named as "black titania", exhibits a bandgap of only 1.85 eV.[15]

The photocatalytic hydrogen formation was studied in H_2O/25 vol % MeOH solutions (10 mL of solution/2.5 mg of catalyst) under vis/NIR light radiation (calibrated 100 W halogen lamp LSK 113 LOT-Oriel GmbH & Co; power density was 0.5 $W{\cdot}cm^{-2}$ at the position of the reactor) using a continuous argon flow setup (20−25 $mL{\cdot}min^{-1}$ of Ar) shown in the Supporting Information (Figure S2). Aqueous solutions of methanol are frequently applied as a test system that confirms the potential of catalysts for hydrogen production.[16] The spectral output of the halogen lamp used in most of experiments matches fairly well the vis/NIR part of the solar spectrum (Figure S5). Some experiments were performed with a RPR 100 device (The Southern New England Ultraviolet Company, P = 11.4 W, $\lambda_{max} \sim$ 575 nm, power density was 0.05 $W{\cdot}cm^{-2}$) using the same composition of photolyte. The specific absorbed power of 0.38 and 0.05 $W{\cdot}mL^{-1}$ for LSK 113 and RPR 100 lamps, respectively, was estimated using the reactor geometry and the volume of irradiated solution as described in the Supporting Information.

Figure 5 demonstrates a typical H_2 emission profile measured by a quadrupole mass spectrometer. Table 1 summarizes the evolution rates (W_{H_2}) and the apparent energetic yields of hydrogen (G_{H_2}) obtained at different experimental conditions. It is noteworthy that no formation of CO_2, CO, or CH_4 was detected in our experiments (Figure S7). Furthermore, the passivated Ti does not exhibit any photocatalytic activity, whatever the experimental conditions, indicating that the presence of crystallized TiO_2 shell is required for hydrogen formation.

It is interesting that for Ti@TiO_2 particles, the highest W_{H_2} value is observed under joint action of light and heat. Moreover, vis/NIR light is much more effective than visible light only. The

DOI: 10.1021/acscatal.5b01401
ACS Catal. 2015, 5, 4790−4795

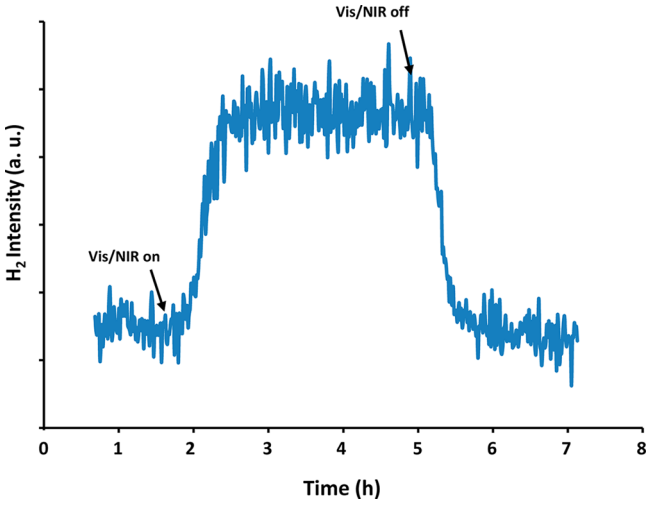

Figure 5. Profile of H_2 evolution under irradiation of the H_2O/25 vol % MeOH (10 mL)/Ti@TiO_2 (2.5 mg) system by vis/NIR light at 60 °C measured by a quadrupole mass spectrometer at a continuous argon flow of 24 mL·min^{-1}.

Table 1. Influence of Experimental Conditions on Hydrogen Evolution Rate[a]

catalyst	irradiating light	T, °C	W_{H_2} μL·min^{-1}·g^{-1}	G_{H_2}[b] μL·min^{-1}·g^{-1}·J^{-1}
Ti	vis/NIR[c]	60	<1	–
Ti@TiO_2	dark conditions[d]	60	<1	–
Ti@TiO_2	vis/NIR	60	174 ± 30	2.7
Ti@TiO_2	vis/NIR	50	140 ± 20	2.0
Ti@TiO_2	vis/NIR	35	96 ± 20	1.3
Ti@TiO_2	vis[e]	35	15 ± 2	0.08

[a]2.5 mg catalyst/10 mL 25 vol % MeOH–H_2O under Ar bubbling. Each W_{H_2} value was averaged from three parallel runs. [b]The G_{H_2} values were calculated taking into account the light absorption of Ti@TiO_2 particles in MeOH-H_2O colloidal suspensions (Figure S8). [c]λ_{max} = 800–850 nm (Figure S5). [d]Commercial pristine anatase (S_{BET} = 71 m^2·g^{-1}, U.S. Research Nanomaterials) studied for comparison also does not exhibit any catalytic activity under these conditions. [e]λ_{max} = 575 nm, no emission at λ > 700 nm (Figure S6).

latter phenomenon could be attributed to much stronger light intensity of a vis/NIR lamp compared with a vis lamp. The positive effect of the light intensity on quantum efficiency has been reported for the photocatalytic ethylene epoxidation in the presence of alumina-supported Ag nanocubes.[17] Table 1 demonstrates that a simple heating of the reaction mixture to 60 °C under dark conditions is insufficient to produce hydrogen in the studied system. On the other hand, a decrease in the bulk temperature from 60 to 35 °C causes a significant drop in the W_{H_2}, even under vis/NIR photolysis.

The kinetics of H_2 generation convincingly indicates the strong photothermal catalytic activity of Ti@TiO_2 nanoparticles. A similar effect reported recently for nonplasmonic noble metal nanoparticles (Pd, Pt, Rh, Ir) in the Suzuki–Miyaura, Hiyama, and Buchwald–Hartwig cross-coupling reactions has been attributed to the metal interband photoexcitation.[18] However, these nanoparticles do not absorb light in the NIR spectral range. Consequently, their photocatalytic performance decreased sharply at higher wavelengths of the incident light, in contrast to Ti@TiO_2 nanoparticles. It is known that the nanorods of some metals (Au, Au/Ag) exhibit photocatalytic activity under NIR light irradiation because of the plasmon-assisted transformation of photon flux energy to energetic electrons, providing enhanced chemical reactivity.[19−22] However, according to Figure 3 titanium nanoparticles do not exhibit a distinguishable plasmon band in the studied vis/NIR spectral range. These results lead us to suggest that the observed photocatalytic effect is most likely due to the electron excitation of the Ti core through interband electronic transitions.

It is noteworthy that the thermally induced catalytic MeOH decomposition can be excluded from consideration at our conditions for two principal reasons. At first sight, the catalytic decomposition of MeOH over TiO_2 is known to occur at 200–300 °C.[23] This is much higher than the temperature in our experiments (35–60 °C). At second glance, catalytic MeOH decomposition should be accompanied by CO emission; however, mass-spectrometric measurements (Figure S7) do not confirm formation of this product. The absence of catalytic activity of pristine TiO_2 at 60 °C (Table 1) also indicates the photocatalytic origin of H_2 emission in the presence of Ti@TiO_2 nanoparticles.

To identify the reaction pathway leading to hydrogen formation, the photocatalytic experiments were performed employing D_2O/25 vol % MeOH solutions. The mass spectra (Figure S9) reveal that the evolved hydrogen is mainly composed of HD and D_2 formed in approximately equal amounts. This result can be understood in terms of the photocatalytic hydrogen formation mechanism developed recently for the aqueous MeOH solutions in the presence of platinized TiO_2 catalyst:[24]

$$CH_3OH + D_2O \leftrightarrow CH_3OD + HOD \quad (1)$$

$$CH_3OD + 2h^+ \rightarrow CH_2O + H^+ + D^+ \quad (2)$$

$$H^+ + e^- \rightarrow H \quad (3)$$

$$D^+ + e^- \rightarrow D \quad (4)$$

$$H + D \rightarrow HD \quad (5)$$

$$CH_2O + D_2O \rightarrow CH_2(OD)_2 \quad (6)$$

$$CH_2(OD)_2 + 2h^+ \rightarrow HCOOH + 2D^+ \quad (7)$$

$$2D^+ + 2e^- \rightarrow D_2 \quad (8)$$

The absence of CO_2 in the outlet gas indicates that photocatalytic decarboxylation of HCOOH does not occur at the studied conditions, most probably because of a large excess of MeOH molecules, which are effectively adsorbed on the active sites of the Ti@TiO_2 particles. Analysis of the irradiated solution using ion chromatography confirmed formation of HCOOH, as is shown in the Supporting Information (Figure S10). At 60 °C, the H_2 formation rate (7.8 μmol·min^{-1}·g^{-1}, vis/NIR lamp, Table 1) is almost twice than that of HCOOH (2.7 μmol·min^{-1}·g^{-1}), in agreement with the mechanism described by eqs 1–8.

The temperature dependence of the studied process leading to H_2 evolution can be a consequence of several phenomena. In general, the positive effect of temperature on the photocatalytic reactions in the presence of plasmonic[1,17] and nonplasmonic[18]

DOI: 10.1021/acscatal.5b01401
ACS Catal. 2015, 5, 4790–4795

noble metal nanoparticles is interpreted in terms of the redistribution of the metal electron into higher energy levels and the increase in the relative population of adsorbed reactants in vibrationally excited states with increasing temperature. The photothermal effect can also be related to the energy required for the migration of intermediates at the surface of the catalyst. This factor becomes important for multistage processes. For gold nanorods deposited on a single TiO_2 crystal, the apparent activation energy (E_{act}) in the oxidation of water via the interband transition was found to be 2.5 times larger (28 kJ·mol^{-1}) than for localized surface plasmon resonance (LSPR) excitation (12 kJ·mol^{-1}).[22,25] This was attributed to the delocalization of the hole generated by the metal interband transition, in contrast to locally concentrated holes in the case of LSPR.[22] In fact, more energy is required for migration of the intermediates in the case of a delocalized hole, which leads to an increase in the E_{act}. The apparent activation energy estimated for Ti@TiO_2 (Table 1), presuming Arrhenius behavior at 35−60 °C (E_{act}= 17 ± 4 kJ·mol^{-1}), is somewhat lower than the E_{act} of the above referred water photolysis induced by interband transition, which may be attributed to the difference in the chemical origin of the intermediates generated in these processes. The quite low E_{act} value assumes that the thermal effect of H_2 generation with the Ti@TiO_2 photocatalyst is governed by migration of the intermediates rather than by the vibrational excitation of the reactant molecules adsorbed at the surface of the catalyst because the temperature effect of the latter process is expected to be much stronger.[1,17,18]

The experimental results lead us to suggest that the driving force of the studied photocatalytic H_2 production with Ti@TiO_2 nanoparticles consists of the Ti core interband transition excitation followed by the formation of energetic electron−hole pairs through nonradiative Landau damping. The nonradiative decay of the collective excitation is widely used to explain the photocatalytic activity of plasmonic metal nanoparticles.[26,27] A recent finding of the significant photocatalytic activity for nonplasmonic noble metal nanoparticles[18] presumes that in a reactive environment, this mechanism is also possible for the interband transitions. Then formed electrons and holes are accumulated in the metallic Ti core and semiconducting TiO_2 shell, respectively. Such a mechanism raises the question about the electron migration pathway from the core to the reactive sites at the surface of the catalyst. Zeng et al. suggested that the electrons traverse the TiO_2 layer ballistically if its thickness is less than ∼10 nm.[28] In the case of Ti@TiO_2 nanoparticles, the electron transport may occur through the junctions between TiO_2 nanocrystals, which can be seen in the HRTEM images shown in Figures 2b and S11. Scavenging of holes by MeOH molecules produces the intermediates that are transformed into HCOOH and into H^+ ions (reactions 2,7). The H^+ ions would migrate to TiO_2/TiO_2 junctions to be reduced to molecular hydrogen by electrons transferred from the metallic core (reactions 3,4,8). It is interesting to note that the activation energy of the H^+ migration in water calculated using a multiscale empirical valence bond simulation approach (12.9 kJ·mol^{-1})[29] is quite similar to the apparent E_{act} obtained in this work for the photocatalytic H_2 generation.

Finally, the Ti@TiO_2 photocatalyst exhibits a very good stability in the studied environment. ICP−OES analyses of the H_2O/25 vol % MeOH solution in contact with Ti@TiO_2 particles at least 1 month and used in several photocatalytic tests revealed the absence (<0.1 ppm) of soluble titanium species. In addition, any modification of the morphology of the particles has been detected after hydrogen evolution experiments. By contrast, similar experiment with air-passivated Ti particles yielded ∼0.3 ppm of dissolved titanium, indicating their lower corrosion resistance compared with Ti@TiO_2.

In conclusion, we have demonstrated a facile synthesis of stable core−shell nanoparticles Ti@TiO_2 using simultaneous actions of ultrasound and hydrothermal treatment on air-passivated titanium nanoparticles in pure water. We have found that Ti@TiO_2 is composed of quasi-spherical metallic titanium particles (20−80 nm) coated by 5−15 nm crystals of defect-free anatase. The obtained material displayed an extended photo response from the UV to the NIR light region as a result of the light absorption by the metallic Ti core. The Ti@TiO_2 nanoparticles revealed high photocatalytic activity in H_2 production from aqueous methanol solutions in the absence of any noble metals. Moreover, the best catalytic performance was observed under the joint effect of vis/NIR light and heat. Isotopic measurement of hydrogen released from a CH_3OH−D_2O mixture pointed out that over the Ti@TiO_2 photocatalyst, methanol acts as a sacrificial reagent for H_2 production, similar to platinized TiO_2 studied recently. At a high concentration of methanol, photocatalytic H_2 formation caused accumulation of HCOOH in the irradiated solution without the release of CO_2, CO, and CH_4 into the gas phase. We have suggested that the reaction mechanism involves accumulation of electron holes in the semiconducting TiO_2 shell via a charge separation that follows the photoexcitation of the Ti interband transitions. The electron transport from the Ti core to the reaction sites at the surface of the catalyst probably occurs through the junctions between TiO_2 crystals of the nanocrystalline shell.

■ ASSOCIATED CONTENT

Supporting Information

The Supporting Information is available free of charge on the ACS Publications website at DOI: 10.1021/acscatal.5b01401.

Experimental details, TGA/DSC curves, the emission spectra of LSK 113 and RPR 100 lamps, and mass spectrometric data for formationof the gaseous products (PDF)

■ AUTHOR INFORMATION

Corresponding Author

*E-mail: serguei.nikitenko@cea.fr.

Notes

The authors declare no competing financial interest.

■ ACKNOWLEDGMENTS

We gratefully acknowledge S. Nitsche for help in the TEM measurements, B. Corso for XRD, C. Rey for TGA/DSC, and P. Pochon and D. Sans for ion chromatography analysis.

■ REFERENCES

(1) Linic, S.; Christopher, P.; Ingram, D. B. *Nat. Mater.* **2011**, *10*, 911−921.

(2) Teoh, W. Y.; Scott, J. A.; Amal, R. *J. Phys. Chem. Lett.* **2012**, *3*, 629−639.

(3) Maeda, K.; Domen, K. *J. Phys. Chem. Lett.* **2010**, *1*, 2655−2661.

(4) Ma, Y.; Wang, X.; Jia, Y.; Chen, X.; Han, H.; Li, C. *Chem. Rev.* **2014**, *114*, 9987−10043.

(5) Serpone, N.; Lawless, D.; Khairutdinov, R.; Pelizzetti, E. *J. Phys. Chem.* **1995**, *99*, 16655−16661.

DOI: 10.1021/acscatal.5b01401
ACS Catal. 2015, 5, 4790−4795

(6) Chen, X.; Liu, L.; Yu, P. Y.; Mao, S. S. *Science* **2011**, *331*, 746−750.
(7) Zuo, F.; Bozhilov, R.; Dillon, I.; Wang, L.; Smith, P.; Zhao, X.; Bardeen, C.; Feng, P. *Angew. Chem., Int. Ed.* **2012**, *51*, 6223−6226.
(8) Zhou, W.; Li, W.; Wang, J.-Q.; Qu, Y.; Yang, Y.; Xie, Y.; Zhang, K.; Wang, L.; Fu, H.; Zhao, D. *J. Am. Chem. Soc.* **2014**, *136*, 9280−9283.
(9) Hirakawa, T.; Kamat, P. V. *J. Am. Chem. Soc.* **2005**, *127*, 3928−3934.
(10) Pihosh, Y.; Turkevych, I.; Mawatari, K.; Fukuda, N.; Ohta, R.; Tosa, M.; Shimamura, K.; Villora, E. G.; Kitamori, T. *Nanotechnology* **2014**, *25*, 315402.
(11) Cau, C.; Guari, Y.; Chave, T.; Larionova, J.; Pochon, P.; Nikitenko, S. I. *J. Phys. Chem. C* **2013**, *117*, 22827−22833.
(12) Ageev, N. V.; Babareko, A. A.; Rubina, E. B.; Betsofen, S. Y.; Bunin, L. A. *Met. Sci. Heat Treat.* **1976**, *18*, 124−130.
(13) Johnson, P. B.; Christy, R. W. *Phys. Rev. B* **1974**, *9*, 5056−5070.
(14) López, R.; Gómez, R. *J. Sol-Gel Sci. Technol.* **2012**, *61*, 1−7.
(15) Naldoni, A.; Allieta, M.; Santangelo, S.; Marelli, M.; Fabbri, F.; Cappelli, S.; Bianchi, C. L.; Psaro, R.; Dal Santo, V. *J. Am. Chem. Soc.* **2012**, *134*, 7600−7603.
(16) Shimura, K.; Yoshida, H. *Energy Environ. Sci.* **2011**, *4*, 2467−2481.
(17) Christopher, P.; Xin, H.; Marimuthu, A.; Linic, S. *Nat. Mater.* **2012**, *11*, 1044−1050.
(18) Sarina, S.; Zhu, H.-Y.; Xiao, Q.; Jaatinen, E.; Jia, J.; Huang, Y.; Zheng, Z.; Wu, H. *Angew. Chem., Int. Ed.* **2014**, *53*, 2935−2940.
(19) Adleman, J. R.; Boyd, D. A.; Goodwin, D. G.; Psaltis, D. *Nano Lett.* **2009**, *9*, 4417−4423.
(20) Christopher, P.; Xin, H.; Linic, S. *Nat. Chem.* **2011**, *3*, 467−472.
(21) Abdulla-Al-Mamun, Md.; Kusumoto, Y.; Zannat, T.; Shariful Islam, Md. *Phys. Chem. Chem. Phys.* **2011**, *13*, 21026−21034.
(22) Nishijima, Y.; Ueno, K.; Kotake, Y.; Murakoshi, K. K.; Inoue, H.; Misawa, H. *J. Phys. Chem. Lett.* **2012**, *3*, 1248−1252.
(23) Usami, Y.; Kagawa, K.; Kawazoe, K.; Matsumura, Y.; Sakurai, H.; Haruta, M. *Appl. Catal., A* **1998**, *171*, 123−130.
(24) Kandiel, T. A.; Ivanova, I.; Bahnemann, D. W. *Energy Environ. Sci.* **2014**, *7*, 1420−1425.
(25) Nishijima, Y.; Ueno, K.; Yokota, Y.; Murakoshi, K.; Misawa, H. *J. Phys. Chem. Lett.* **2010**, *1*, 2031−2036.
(26) Linic, S.; Aslam, U.; Boerigter, C.; Morabito, M. *Nat. Mater.* **2015**, *14*, 567−576.
(27) Kale, M. J.; Avanesian, T.; Christopher, P. *ACS Catal.* **2014**, *4*, 116−128.
(28) Zeng, G.; Qiu, J.; Li, Z.; Pavaskar, P.; Cronin, S. B. *ACS Catal.* **2014**, *4*, 3512−3516.
(29) Chen, H.; Voth, G. A.; Agmon, N. *J. Phys. Chem. B* **2010**, *114*, 333−339.

DOI: 10.1021/acscatal.5b01401
ACS Catal. 2015, 5, 4790−4795